NANO LETTERS

Letter

pubs.acs.org/NanoLett

Four-Wave Mixing in Landau-Quantized Graphene

Jacob C. König-Otto,[*,†,‡] Yongrui Wang,[§] Alexey Belyanin,[§] Claire Berger,[∥,⊥] Walter A. de Heer,[∥] Milan Orlita,[#,▽] Alexej Pashkin,[†] Harald Schneider,[†] Manfred Helm,[†,‡] and Stephan Winnerl[†]

[†]Helmholtz-Zentrum Dresden-Rossendorf, P.O. Box 510119, 01314 Dresden, Germany

[‡]Technische Universität Dresden, 01062 Dresden, Germany

[§]Texas A&M University, College Station, Texas 77843-4242, United States

[∥]Georgia Institute of Technology, Atlanta, Georgia 30332, United States

[⊥]Institut Néel, CNRS-Université Alpes, 38042 Grenoble, France

[#]LNCMI, CNRS-UGA-UPS-INSA, 38042 Grenoble, France

[▽]Institute of Physics, Charles University in Prague, 12116 Prague, Czech Republic

ABSTRACT: For Landau-quantized graphene, featuring an energy spectrum consisting of nonequidistant Landau levels, theory predicts a giant resonantly enhanced optical nonlinearity. We verify the nonlinearity in a time-integrated degenerate four-wave mixing (FWM) experiment in the mid-infrared spectral range, involving the Landau levels LL_{-1}, LL_0 and LL_1. A rapid dephasing of the optically induced microscopic polarization on a time scale shorter than the pulse duration (~4 ps) is observed, while a complementary pump−probe experiment under the same experimental conditions reveals a much longer lifetime of the induced population. The FWM signal shows the expected field dependence with respect to lowest order perturbation theory for low fields. Saturation sets in for fields above ~6 kV/cm. Furthermore, the resonant behavior and the order of magnitude of the third-order susceptibility are in agreement with our theoretical calculations.

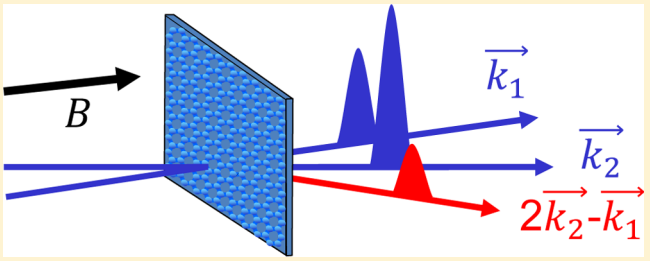

KEYWORDS: *Graphene, four-wave mixing, nonlinear optics, Landau-quantization*

Graphene is a two-dimensional material with a gapless linear band structure in the vicinity of two Dirac points. It possesses unique mechanical, electrical, and optical properties, which have led to a high interest in a broad range of fields. An example for those outstanding features are the highly nonlinear optical properties of graphene in a wide spectral range from terahertz (THz) frequencies to visible light. The third-order nonlinear optical response has been investigated theoretically, both on a semiclassical and on a fully quantum mechanical basis.[1−7] In the latter case, in particular the four-wave mixing (FWM) process is addressed. Experimentally FWM signals have been observed in the near-infrared spectral range[7−12] and third-order nonlinear susceptibilities have been found to be in the order of $\chi^{(3)} \sim 10^{-25}$−10^{-23} m^3/V^2. At THz frequencies however, only pump−probe signals, but no FWM signals, have been found.[13] When a magnetic field is applied perpendicular to the graphene layer the linear dispersion of graphene breaks up into a series of nonequidistant Landau levels.[14] This offers the possibility to resonantly enhance the nonlinear-optical response and to tune the resonance frequency by adjusting the strength of the magnetic field. Recently, a giant nonlinear-optical response ($\chi^{(3)} \sim 10^{-19}$ m^3/V^2) has been predicted for Landau-quantized graphene.[15,16] In this Letter, we present the first experimental investigation of this effect by studying transient, degenerate FWM. To this end, the $LL_{-1} \rightarrow LL_0$ and $LL_0 \rightarrow LL_1$ transitions are excited resonantly with radiation at 19 THz (78 meV). The experimental findings are in good agreement with our theoretical calculations based on the density-matrix formalism.

A multilayer epitaxial graphene sample (~50 layers) produced by thermal decomposition of SiC on the C-face of 4H-SiC is used in the experiments.[17] Although the amount of graphene layers formed on the SiC substrate is large, the different layers behave like single layer graphene, because they are electronically decoupled.[18,19] The Fermi level in the different graphene layers is determined by polarization doping of the substrate.[20] The majority of layers is slightly n-doped and only the layers at the interface to SiC exhibit a stronger doping[21] and are therefore transparent at the used photon energy of 78 meV and a magnetic field of 4.5 T. The sample is kept in a split-coil superconducting magneto-cryostat at a temperature of 10 K in a cold helium gas atmosphere. The scheme of the experimental setup is depicted in Figure 1. The laser pulses from the free-electron laser FELBE are split into two separate paths and are focused with an off-axis parabolic mirror onto the sample inside the magneto-cryostat. A time

Received: November 8, 2016
Revised: February 24, 2017
Published: February 24, 2017

DOI: 10.1021/acs.nanolett.6b04665
Nano Lett. 2017, 17, 2184−2188

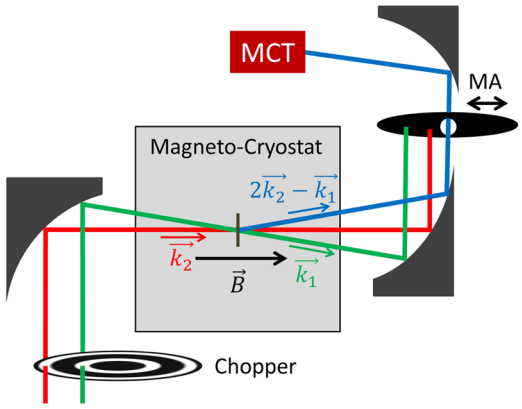

Figure 1. Experimental setup. The movable aperture (MA) is used to select the FWM signal in direction $2\vec{k}_2-\vec{k}_1$ or to measure a pump−probe signal in $\vec{k}_1$ direction with the MCT detector.

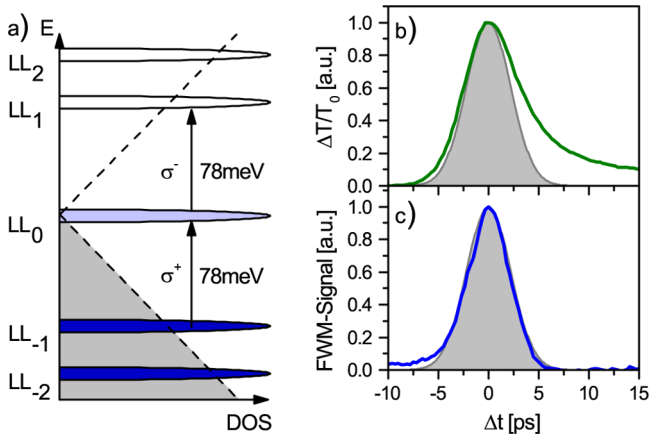

Figure 2. (a) The magnetic field of 4.5 T leads to a Landau-quantization in the graphene sample, whereas the transition from LL_{-1} (LL_0) to LL_0 (LL_1) is resonant to the photon energy of 78 meV. (b) The transient change in population is recorded by a degenerate pump−probe experiment, measuring the transient change of transmission of $\vec{k}_1$ (field: 6 kV/cm) caused by the absorption of $\vec{k}_2$ (field: 12 kV/cm). (c) The microscopic polarization is probed by detecting the FWM signal $2\vec{k}_2-\vec{k}_1$ at the same incident fields. The shaded areas show the autocorrelation of the laser pulses calculated from spectra.

delay Δt between the two pulses can be controlled with a motorized delay stage (not shown). The beams in direction $\vec{k}_1$, $\vec{k}_2$ and the FWM signal in direction $2\vec{k}_2-\vec{k}_1$ are simultaneously collimated by a second parabolic mirror. A movable aperture is used to select which beam is detected by the nitrogen cooled mercury−cadmium−telluride (MCT) detector. Both incident beams are modulated by a dual-slot optical chopper and the signals are detected by a lock-in amplifier at the sum of the modulation frequencies for both beams. This enables one to suppress a time-independent background caused by stray light.

If the sample is brought into a magnetic field of around 4.5 T with a direction perpendicular to the surface, the band structure of graphene breaks up into a system of Landau levels and the $LL_{-1} \rightarrow LL_0$ and $LL_0 \rightarrow LL_1$ transitions become resonant with the photon energy of 78 meV. For the almost intrinsic graphene layers LL_{-1} is fully occupied, LL_0 close to half filling and LL_1 is completely empty. In detail, we expect the filling of the zeroth Landau-level to be in the order of 0.52 at this magnetic field (corresponding to a carrier concentration of 8×10^9 cm^{-2} at zero field[22]). In this work, both incident pulses are linearly polarized in the same direction. Thus, the excitation of both transitions is possible as indicated in Figure 2a. The transient change in transmission $\Delta T/T_0$ of the sample due to strong optical excitation is depicted in Figure 2b. For this kind of measurement, the movable aperture is set to transmit the $\vec{k}_1$ beam and the transient change in transmission of this beam caused by the absorption of photons from the $\vec{k}_2$ beam is recorded. The pump−probe signal features a fast decay and a slower component in the order of several hundreds of picoseconds. Recent studies already gave first insight into the population dynamics of this system.[23−26] In particular, a rapid (faster than pulse duration of ∼4 ps) depopulation of an optically pumped level via Auger scattering has been observed.[26] This Coulomb process leads to a fast thermalization of electrons. The slower time scale of the decay is attributed to cooling of the electronic system via phonon scattering.

While the pump−probe signal corresponds mostly to Pauli blocking and reveals the dynamics of the excited population, the FWM signal is sensitive to the induced polarization in the sample. The decay of the microscopic polarization is governed both by the relaxation of the population and by pure dephasing processes. In our FWM experiment, the $\vec{k}_1$ beam in direction $\vec{k}_1$ induces a polarization in the sample. The $\vec{k}_2$ beam, arriving after the delay time Δt, interferes with the remnant $\vec{k}_1$ polarization and creates a polarization grating with the wave vector $\vec{k}_2-\vec{k}_1$. The second part of the $\vec{k}_2$ beam gets diffracted by this grating in the direction $2\vec{k}_2-\vec{k}_1$. Thus, the decay time of the FWM signal is defined by the polarization dephasing processes and not by the population decay. Figure 2c depicts the FWM signal at the very same experimental conditions as for the pump−probe signal in Figure 2b. Comparing both types of signals one can see some clear differences. The FWM signal is basically symmetric apart from a small artifact, namely a baseline offset at negative delay times, which stems from pump−probe signals that are scattered as stray light into the detector. Note that the time delay relevant for the FWM signal is inverted with respect to the pump−probe signal.[27] The FWM signal is only observed during the temporal overlap of the pulses, indicating that the dephasing time is considerably shorter than the temporal resolution of our experiment set by the pulse duration of around ∼4 ps. This result, together with the previous detailed study of the population dynamics,[26] suggests that Auger processes within the LL_{-1}, LL_0, and LL_1 subset of Landau levels cause a rapid dephasing of the microscopic polarization.

Next, we investigate the dependence of the FWM process on the electric fields of the beams in $\vec{k}_1$ and $\vec{k}_2$ direction. The electric field of the generated FWM signal can be estimated from the induced third-order polarization, which depends on the third-order nonlinear surface (2D) susceptibility $\chi^{(3)}$ (in SI units) and is given by

$$|\vec{E}_{\mathrm{FWM}}| \simeq \frac{\omega}{2c}|\chi^{(3)}E^2(\vec{k}_2)E(\vec{k}_1)| \quad (1)$$

Here ω is the frequency, $E(\vec{k}_1)$ and $E(\vec{k}_2)$ the fields of the incident beams, and c is the velocity of light. The surface susceptibility $\chi^{(3)}$ for this process is a function of the magnetic field and the photon energy itself. We will have a closer look on this in the next section. Equation 1 indicates that the FWM field scales linearly with the field of the beam in direction $\vec{k}_1$ and quadratically with the field of the beam in direction $\vec{k}_2$. Thus, if the field of both beams is tuned simultaneously, the FWM field should scale cubically. For a variety of different field

DOI: 10.1021/acs.nanolett.6b04665
Nano Lett. 2017, 17, 2184−2188

combinations of the two incident beams, FWM transients were recorded and the maxima of the transients were extracted. The incident peak fields were determined from the measured power, spot size and pulse duration. To determine E_{FWM} one has to consider the losses at the movable aperture and the calibration of the MCT detector additionally. Note that the inaccuracy of this procedure has no influence on the determined scaling behavior of the FWM field with respect to the incident fields. The quantitative values of the FWM field, however, are expected to be accurate only within a factor of 3, since the determined FWM intensities are estimated to be accurate within 1 order of magnitude. The FWM peak fields are plotted in Figure 3 as a function of the peak field of the beam in $\vec{k}_2$

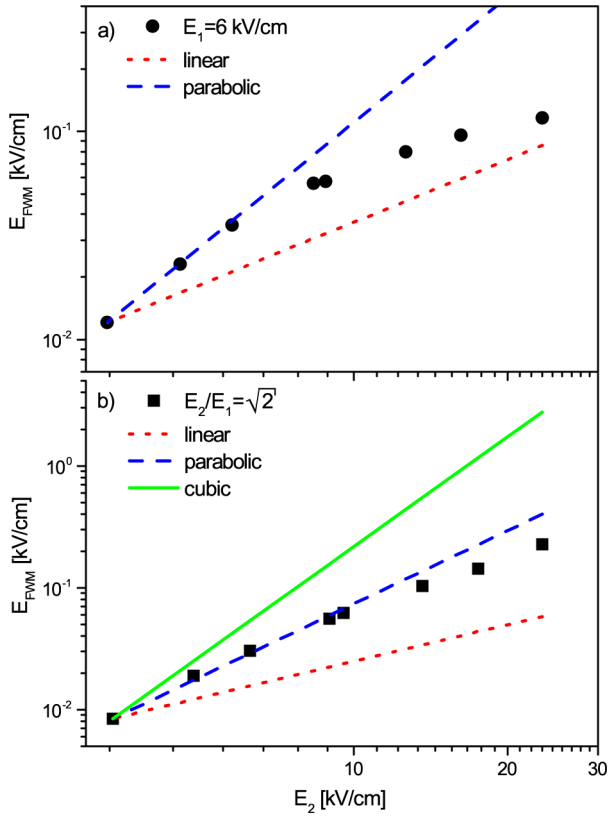

Figure 3. Saturation behavior of the FWM signal. (a) The field of beam one is kept at 6 kV/cm, while the field from beam two is varied. (b) Both fields are varied while keeping a constant ratio of $\sqrt{2}$.

direction. Figure 3a shows the field dependence when the field of the $\vec{k}_1$ beam is kept constant at 6 kV/cm (corresponding to a fluence of ~0.2 μJ/cm^2) and only the field of the $\vec{k}_2$ beam is varied. Linear and quadratic power laws are indicated by the dotted red and blue dashed line, respectively. The three lowest data points are in agreement with a quadratic dependence. Note that in the case of a pump−probe signal one would only expect a linear scaling of the signal. This, together with the different temporal shapes of the signals (see Figure 2), allows one to clearly identify the FWM signal and distinguish it from potential stray pump−probe signals. Nevertheless, a clear saturation is noticeable in the measured field regime. A deeper analysis of saturation effects is beyond the scope of this work. However, in ref 16 saturation fields are calculated for FWM processes with a different level scheme in Landau-quantized graphene under continuous excitation. Despite the differences of the processes evaluated in this work and in ref 16, the reported saturation behavior can serve as an estimation for the order of magnitude of the saturation field. For a magnetic field of 4.5 T and a dephasing time of 190 fs (this value is discussed later in this Letter), the saturation field is in the order of 4 kV/cm, which is consistent with the experiment, where a deviation from the square root dependence is observed for fields higher than 6 kV/cm. Pump−probe measurements under comparable conditions feature a saturation at comparable pumping fields, indicating that the observed saturation in the FWM experiment might be explained due to band filling.

In accord with the consideration that two photons of the beam in $\vec{k}_2$ direction interact with one photon of the beam in $\vec{k}_1$ direction, it is reasonable to choose a ratio of the two fields of $E_2/E_1 \approx \sqrt{2}$. The strength of the FWM signal for this constant ratio is depicted Figure 3b. Again the straight lines represent different power laws. The data points do not follow the green line that represents the expected cubic dependence of this case. However, the dependence is found to be superquadratic for the low fields. The observed saturation is not surprising. From Figure 3a, one can see that at the measured fields already the parabolic dependence on E_2 saturates. Saturation naturally occurs faster if both fields are varied. It was not possible to achieve sufficient signal-to-noise ratio at lower fields to clearly demonstrate the cubic dependence.

In the following, the resonant behavior of the FWM signal is studied by measuring transients at different magnetic fields, while keeping the photon energy fixed. In Figure 4 the peak

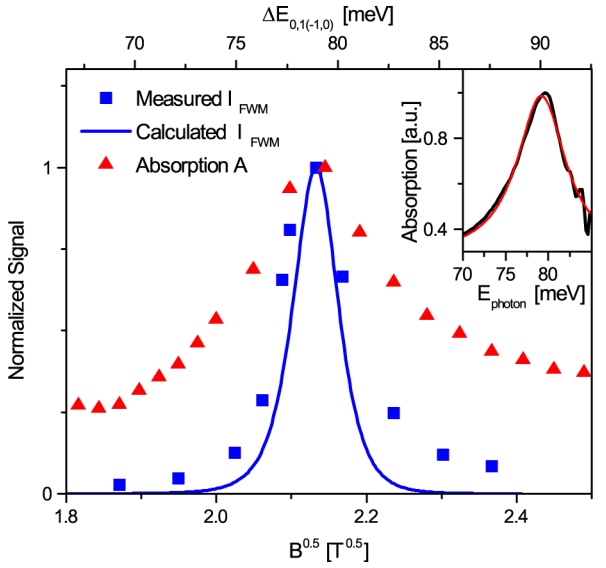

Figure 4. Linear absorption (red triangles) and maxima of FWM mixing signals (blue squares) for different magnetic fields. The field of beam two is 12 kV/cm and beam one 5.3 kV/cm. The blue line shows the calculated magnetic field dependency of the $\chi^{(3)}$ process. The inset shows a Lorentzian fit to the linear absorption spectra at 4.5 T to determine the line broadening.

FWM intensities are plotted on a $\sqrt{B}$-scale, that is, a scale that is linear in the energy of the optical transition $LL_{-1} \rightarrow LL_0$ and $LL_0 \rightarrow LL_1$.[14] Additionally the linear absorption measured by Fourier transform spectroscopy, as described by Orlita et al. in ref 28, is shown. One can clearly see that the resonance of the $\chi^{(3)}$ process is much narrower as compared to the linear absorption. As mentioned before, the dependence of the FWM signal on the magnetic field stems from the nonlinear

DOI: 10.1021/acs.nanolett.6b04665
Nano Lett. 2017, 17, 2184−2188

susceptibility $\chi^{(3)}$. We derive an expression for $\chi^{(3)}$ using the density-matrix formalism similarly to refs 15 and 16. Here we only consider transitions that are close to resonance with the pump fields. By using this approximation, the linear and second-order density matrix elements are solely determined by the pump field E_2, while the field E_1 only enters the third-order density matrix elements. For our specific case, that is, two incident fields with the same linear polarization, and under the assumption of equal line broadening factors for the different transitions, the surface susceptibility can be written as

$$\chi^{(3)}(\omega, 2\vec{k}_2 - \vec{k}_1) = \frac{1}{2\pi l_c^2 \hbar^3 \epsilon_0} \frac{e^4 v_f^4}{\omega \omega_c^3} \frac{i}{\omega + i\gamma - \omega_c} \times \frac{1}{2(2\omega + i\gamma - 2\omega_c)} \frac{(\rho_{-1} - \rho_0) - (\rho_0 - \rho_1)}{\omega + i\gamma - \omega_c} \quad (2)$$

Here v_f is the Fermi velocity in graphene, $\omega_c = v_f\sqrt{\frac{2eB}{\hbar}}$ is the resonance frequency, $l_c = \sqrt{\frac{\hbar}{eB}}$ the magnetic length, ρ_i is the occupation of the LL_i and γ is the line broadening. The numerator of the last fraction is in our case approximately −0.04, because of the small doping. For intrinsic graphene $\chi^{(3)}$ would vanish in this configuration since contributions from the transitions $LL_{-1} \rightarrow LL_0$ and $LL_0 \rightarrow LL_1$ cancel each other. This reflects electron−hole symmetry of intrinsic graphene. The line broadening for the calculation was taken from the linear absorption measurement by applying a Lorentzian fit to the absorption line (see inset in Figure 4), which yielded $\gamma \simeq 3.5$ meV. Note that this corresponds to a total dephasing time of $\tau = \hbar/\gamma = 190$ fs, assuming a homogeneously broadened line. The fact that the decay of the FWM signal was faster than the pulse duration of 4 ps is consistent with this number. The experimental FWM resonance appears to be slightly broader than the calculated one (see Figure 4). This may have two possible reasons. First, eq 2 does not account for saturation effects. Taking them into account will broaden the calculated peak. Second, in fact, both Landau-level populations and relaxation rates in eq 2 can be viewed as time-dependent during the pulse. An increasing field amplitude of the incident pulse leads to an increase in the amount of nonequilibrium carriers and an accelerated Auger recombination, which has a strongly nonlinear dependence on the nonequilibrium carrier density. These effects contribute to the saturation of the FWM signal strength and an enhanced broadening of the FWM resonance. Furthermore, far away from the resonance the effect of scattered stray light is more dominant, as the pump−probe signal possesses a broader resonance. Consequently, the strength of the experimental FWM signal may be overestimated in the nearly off-resonant case.

It is instructive to compare the dephasing time estimated from the broadening of the LLs to scattering times discussed in literature. The latter are primarily momentum relaxation times obtained from transport measurements. In the simplest approach, the momentum relaxation time τ_m is related to the carrier mobility by the expression[29] $\mu = e\tau_m v_f^2/E_f$. From this expression, relaxation times of 4 and 50 fs can be extracted from quantum Hall effect measurements on monolayer graphene on the Si face of SiC and monolayer quasi-free-standing graphene prepared by hydrogen intercalation on the Si face of SiC, respectively.[30,31] It has been pointed out that the momentum relaxation time can differ, depending on the predominant scattering mechanism, by a factor of 1−5 from the time constant related to the quantum level broadening.[32] Typical values for the level broadening of exfoliated graphene on SiO_2 are in the range from 30−50 fs,[32] approximately three times higher values are found in graphene on hBN.[33] The comparably high value of 190 fs for our sample indicates the high structural quality. Finally we note that extremely pure graphene on graphite layers exhibit dephasing times of up to 20 ps.[34]

Finally, we discuss the strength of the $\chi^{(3)}$-process. According to eq 2, one layer of graphene with $\rho_0 = 0.52$ in a magnetic field resonant to the photon energy features a surface susceptibility of 4.9×10^{-20} m^3/V^2. This corresponds to a bulk susceptibility of 1.6×10^{-10} m^2/V^2, assuming a layer thickness of 0.3 nm. For comparison with the experiment, it is reasonable to select one of the lower excitation data points from Figure 3a, where the saturation is negligible. From the second point, where the incoming fields are set to $E_2 = 4.6$ kV/cm and $E_1 = 5.9$ kV/cm and $E_{FWM} = 0.023$ kV/cm is measured, we derive $\chi^{(3)} \sim 9.2 \times 10^{-20}$ m^3/V^2 using eq 1. Note that the experimental value is not the $\chi^{(3)}$ for one single layer of graphene, as our sample consists of roughly 50 layers. Considering the uncertainty in the experimental determination of E_{FWM}, experiment and theory are in reasonable agreement. For doped graphene, where the zeroth Landau-level is either completely filled or empty at a magnetic field of several Tesla, a much higher susceptibility is expected, as the numerator in eq 2 will be 25 times higher (i.e., $\chi^{(3)} \sim 10^{-18}$ m^3/V^2). Considering the small thickness of graphene, this is in fact a strong nonlinearity. The surface susceptibility of Landau-quantized graphene is comparable to the value observed for intersubband transitions in GaAs quantum wells with much larger thickness and 2D electron density. For example, the intersubband transition at 124 meV in a GaAs/AlGaAs superlattice results in $\chi^{(3)} \sim 1.3 \times 10^{-18}$ m^3/V^2, which is 3 orders of magnitude larger than the intraband nonlinearity due to nonparabolicity of the wells.[35] Coupled-quantum-well structures based on AlInAs/GaInAs are demonstrated with a susceptibility of $\chi^{(3)} \sim 1.4 \times 10^{-20}$ m^3/V^2 measured by third-harmonic generation.[36] Even higher third-order nonlinearities $\chi^{(3)} \sim 5 \times 10^{-17}$ m^3/V^2 are predicted in the THz range by utilizing impurity transitions in GaAs quantum well[37] but have not yet been verified experimentally.

In summary, the proposed large third-order nonlinearity in Landau-quantized graphene is experimentally demonstrated for the first time. The order of $\chi^{(3)}$, the resonance behavior, and the field dependencies are in good agreement with our theoretical predictions. Landau-quantized graphene represents a system with a strong optical nonlinearity and offers spectral tunability by variation of the magnetic field. These properties are attractive for a variety of mid-infrared nonlinear optical applications such as frequency multiplication, parametric generation, and sum-frequency generation.

AUTHOR INFORMATION

Corresponding Author

*E-mail: j.koenig-otto@hzdr.de.

ORCID

Jacob C. König-Otto: 0000-0002-2470-1261

Notes

The authors declare no competing financial interest.

DOI: 10.1021/acs.nanolett.6b04665
Nano Lett. 2017, 17, 2184−2188

■ ACKNOWLEDGMENTS

We thank P. Michel and his team for their dedicated support. This work was financially supported by the SPP 1459 of the DFG and by the EC Graphene Flagship (Project No. 604391).

■ REFERENCES

(1) Mikhailov, S. A.; Ziegler, K. *J. Phys.: Condens. Matter* **2008**, *20*, 384204.
(2) Mikhailov, S. A. *Phys. Rev. B: Condens. Matter Mater. Phys.* **2016**, *93*, 085403.
(3) Cheng, J. L.; Vermeulen, N.; Sipe, J. E. *New J. Phys.* **2014**, *16*, 053014.
(4) Cheng, J. L.; Vermeulen, N.; Sipe, J. E. *Phys. Rev. B: Condens. Matter Mater. Phys.* **2015**, *91*, 235320.
(5) Shareef, S.; Ang, Y. S.; Zhang, C. *J. Opt. Soc. Am. B* **2012**, *29*, 274.
(6) Zhang, Z.; Voss, P. L. *Opt. Lett.* **2011**, *36*, 4569.
(7) Hendry, E.; Hale, P. J.; Moger, J.; Savchenko, A. K.; Mikhailov, S. A. *Phys. Rev. Lett.* **2010**, *105*, 097401.
(8) Ciesielski, R.; Comin, A.; Handloser, M.; Donkers, K.; Piredda, G.; Lombardo, A.; Ferrari, A. C.; Hartschuh, A. *Nano Lett.* **2015**, *15*, 4968.
(9) Rao, S. M.; Lyons, A.; Roger, T.; Clerici, M.; Zheludev, N. I.; Faccio, D. *Sci. Rep.* **2015**, *5*, 15399.
(10) Xia, C. Q.; Zheng, C.; Fuhrer, M. S.; Palomba, S. *Opt. Lett.* **2016**, *41*, 1122.
(11) Xu, B.; Martinez, A.; Yamashita, S. *IEEE Photonics Technol. Lett.* **2012**, *24*, 1792.
(12) Säynätjoki, A.; Karvonen, L.; Riikonen, J.; Kim, W.; Mehravar, S.; Norwood, R. A.; Peyghambarian, N.; Lipsanen, H.; Kieu, K. *ACS Nano* **2013**, *7*, 8441.
(13) Woerner, M.; Kuehn, W.; Bowlan, P.; Reimann, K.; Elsaesser, T. *New J. Phys.* **2013**, *15*, 025039.
(14) Goerbig, M. O. *Rev. Mod. Phys.* **2011**, *83*, 1193.
(15) Yao, X.; Belyanin, A. *Phys. Rev. Lett.* **2012**, *108*, 255503.
(16) Yao, X.; Belyanin, A. *J. Phys.: Condens. Matter* **2013**, *25*, 054203.
(17) Berger, C.; Song, Z.; Li, X.; Wu, X.; Brown, N.; Naud, C.; Mayou, D.; Li, T.; Hass, J.; Marchenkov, A. N.; Conrad, E. H.; First, P. N.; de Heer, W. A. *Science* **2006**, *312*, 1191.
(18) Hass, J.; Varchon, F.; Millán-Otoya, J. E.; Sprinkle, M.; Sharma, N.; de Heer, W. A.; Berger, C.; First, P. N.; Magaud, L.; Conrad, E. H. *Phys. Rev. Lett.* **2008**, *100*, 125504.
(19) Sprinkle, M.; et al. *Phys. Rev. Lett.* **2009**, *103*, 226803.
(20) Mammadov, S.; Ristein, J.; Koch, R. J.; Ostler, M.; Raidel, C.; Wanke, M.; Vasiliauskas, R.; Yakimova, R.; Seyller, T. *2D Mater.* **2014**, *1*, 035003.
(21) Sun, D.; Divin, C. J.; Berger, C.; de Heer, W. A.; First, P. N.; Norris, T. B. *Phys. Rev. Lett.* **2010**, *104*, 136802.
(22) Suess, R. J.; Winnerl, S.; Schneider, H.; Helm, M.; Berger, C.; de Heer, W. A.; Murphy, T. E.; Mittendorff, M. *ACS Photonics* **2016**, *3*, 1069.
(23) Mittendorff, M.; Orlita, M.; Potemski, M.; Berger, C.; de Heer, W. A.; Schneider, H.; Helm, M.; Winnerl, S. *New J. Phys.* **2014**, *16*, 123021.
(24) Plochocka, P.; Kossacki, P.; Golnik, A.; Kazimierczuk, T.; Berger, C.; de Heer, W. A.; Potemski, M. *Phys. Rev. B: Condens. Matter Mater. Phys.* **2009**, *80*, 245415.
(25) Wendler, F.; Knorr, A.; Malić, E. *Nat. Commun.* **2014**, *5*, 4839.
(26) Mittendorff, M.; Wendler, F.; Malic, E.; Knorr, A.; Orlita, M.; Potemski, M.; Berger, C.; de Heer, W. A.; Schneider, H.; Helm, M.; Winnerl, S. *Nat. Phys.* **2014**, *11*, 75.
(27) Yajima, T.; Taira, Y. *J. Phys. Soc. Jpn.* **1979**, *47*, 1620.
(28) Orlita, M.; Faugeras, C.; Plochocka, P.; Neugebauer, P.; Martinez, G.; Maude, D. K.; Barra, A.-L.; Sprinkle, M.; Berger, C.; de Heer, W. A.; Potemski, M. *Phys. Rev. Lett.* **2008**, *101*, 267601.
(29) Tan, Y.-W.; Zhang, Y.; Bolotin, K.; Zhao, Y.; Adam, S.; Hwang, E. H.; das Sarma, S.; Stormer, H. L.; Kim, P. *Phys. Rev. Lett.* **2007**, *99*, 246803.
(30) Shen, T.; Gu, J. J.; Xu, M.; Wu, Y. Q.; Bolen, M. L.; Capano, M. A.; Engel, L. W.; Ye, P. D. *Appl. Phys. Lett.* **2009**, *95*, 172105.
(31) Tanabe, S.; Takamura, M.; Harada, Y.; Kageshima, H.; Hibino, H. *Appl. Phys. Express* **2012**, *5*, 125101.
(32) Hong, X.; Zou, K.; Zhu, J. *Phys. Rev. B: Condens. Matter Mater. Phys.* **2009**, *80*, 241415.
(33) Dean, C. R.; Young, A. F.; Meric, I.; Lee, C.; Wang, L.; Sorgenfrei, S.; Watanabe, K.; Taniguchi, T.; Kim, P.; Shepard, K. L.; Hone, J. *Nat. Nanotechnol.* **2010**, *5*, 722.
(34) Neugebauer, P.; Orlita, M.; Faugeras, C.; Barra, A.-L.; Potemski, M. *Phys. Rev. Lett.* **2009**, *103*, 136403.
(35) Walrod, D.; Auyang, S. Y.; Wolff, P. A.; Sugimoto, M. *Appl. Phys. Lett.* **1991**, *59*, 2932.
(36) Sirtori, C.; Capasso, F.; Sivco, D. L.; Cho, A. Y. *Phys. Rev. Lett.* **1992**, *68*, 1010.
(37) Yıldırım, H.; Aslan, B. *Semicond. Sci. Technol.* **2011**, *26*, 085017.

DOI: 10.1021/acs.nanolett.6b04665
Nano Lett. 2017, 17, 2184−2188